Distributed Robust Energy and Reserve Dispatch for Coordinated Transmission and Active Distribution Systems

Yongli Ji, Qingshan Xu, and Yuanxing Xia

***Abstract*—The increasing penetration of renewable energy sources introduces higher requirements for the operation flexibility of transmission system (TS) and connected active distribution systems (DSs). This paper presents an efficient distributed framework for the TS and DSs to work cooperatively yet independently. In addition to conventional power interaction, upward and downward reserve capacities are exchanged to form the feasible access regions at the boundaries that apply to different system operation situations. A distributed robust energy and reserve dispatch approach is proposed under this framework. The approach utilizes the supply- and demand-side resources in different systems to handle various uncertainties and improve overall efficiency and reliability. In particular, integrated as aggregated virtual energy storage (AVES) devices, air-conditioning loads are incorporated into the optimal dispatch. In addition, a reserve model with charging/discharging-state elasticity is developed for AVESs to enhance system flexibility and provide additional reserve support. Different cases are compared to verify the effectiveness and superiority of the proposed approach.**

***Index Terms*—Air-conditioning load, distributed coordination, feasible access region, interregional energy and reserve support, transmission and active distribution system.**

NOMENCLATURE

A. Superscripts

DS	Variables or parameters of distribution system (DS)
TS	Variables or parameters of transmission system (TS)
u	Variables or parameters in uncertainty cases

B. Sets and Indices

$b_1 \in \mathcal{B}^{TS}$, $b_1 \in \mathcal{B}^{TS}_{b1}$	Sets of nodes and those connected to b_1 in TS
$b_2, j_2 \in \mathcal{B}^{DS}_{d}$, $b_2, j_2 \in \mathcal{B}^{DS}_{d,b2}$	Sets of nodes and those connected to b_2 in DS d
$d \in \mathcal{B}^{con}$	Index for boundary nodes connecting TS and DS (DSs)
$i \in \mathcal{N}_p$	Set of air conditioner (AC) in population p
$l_1 \in \mathcal{L}^{TS}$, $l_2 \in \mathcal{L}^{DS}_{d}$	Sets of lines of TS and DSs d
$m_1 \in \mathcal{G}^{TS}$, $m_1 \in \mathcal{G}^{TS}_{b1}$	Sets of units and those connected to b_1 in TS
$m_2 \in \mathcal{G}^{DS}_{d}$, $m_2 \in \mathcal{G}^{DS}_{d,b2}$	Sets of units and those connected to b_2 in DS d
$p \in \mathcal{VS}_{d}$, $p \in \mathcal{VS}_{d,b2}$	Sets of AC populations and those connected to b_2 in DS d
q, l	Indices of outer and inner recourse variables in compact model
Q, L	Indices of outer and inner iteration of column-and-constraint generation (C&CG) algorithm
$t, \tau \in \mathcal{T}$	Sets of time intervals
$w_1 \in \mathcal{W}^{TS}$, $w_1 \in \mathcal{W}^{TS}_{b1}$	Sets of wind farms and those connected to b_1 in TS
$w_2 \in \mathcal{W}^{DS}_{d}$, $w_2 \in \mathcal{W}^{DS}_{d,b2}$	Sets of wind farms and those connected to b_2 in DS d

C. Parameters

Γ^{D}, Γ^{wind}	Uncertainty budgets of load and wind power
Δt	Interval duration
α^{G}_{m1}, α^{G}_{m2}, β^{G}_{m1}, β^{G}_{m2}, γ^{G}_{m1}, γ^{G}_{m2}	Generation cost coefficients of units
$\boldsymbol{\pi}$	Dual variable of second-stage continuous variable $\boldsymbol{y}$
$\boldsymbol{A}$, $\boldsymbol{B}$, $\boldsymbol{C}$, $\boldsymbol{D}$, $\boldsymbol{E}$, $\boldsymbol{F}$, $\boldsymbol{G}$, $\boldsymbol{H}$, $\boldsymbol{J}$, $\boldsymbol{f}$, $\boldsymbol{g}$	Coefficient matrices in compact model

Manuscript received: July 28, 2022; revised: November 25, 2022; accepted: January 9, 2023. Date of CrossCheck: January 9, 2023. Date of online publication: March 24, 2023.

This work was supported by the Scientific Research Startup Foundation of Recruiting Talents of Nanjing Institute of Technology (No. YKJ202225).

Y. Ji (corresponding author) is with the Smart Grid Research Institute, Nanjing Institute of Technology, Nanjing 211167, China (e-mail: gjfw_5_jyl@163.com).

Q. Xu and Y. Xia are with the School of Electrical Engineering, Southeast University, Nanjing 210096, China (e-mail: xuqingshan@seu.edu.cn; eexyx@seu.edu.cn).

DOI: 10.35833/MPCE.2022.000460

A_p^A, C_p^A Coefficients of aggregated virtual energy storage (AVES)

a_i, b_i, c_i Coefficients of virtual energy storage (VES)

$AVSOC_{p,t}^{\mathrm{MAX}}$ State of charge (SOC)-level upper limits of AVESs

C, R Equivalent thermal capacitance and resistance

$C_p^{AVES,ch}$, $C_p^{AVES,dis}$ Charging and discharging costs of AVESs

$C_p^{AVES,ch,up}$, $C_p^{AVES,ch,dn}$ Up- and down-charging reserve costs of AVESs

$C_p^{AVES,dis,up}$, $C_p^{AVES,dis,dn}$ Up- and down-discharging reserve costs of AVESs

C_{curt}^{D}, C_{curt}^{wind} Load shedding and wind curtailment costs

$C_{m1}^{G,up}$, $C_{m2}^{G,up}$, $C_{m1}^{G,dn}$, $C_{m2}^{G,dn}$ Upward and downward reserve costs of units

C_{m1}^{SU}, C_{m2}^{SU}, C_{m1}^{SD}, C_{m2}^{SD} Start-up and shut-down costs of units

$\boldsymbol{d}^{(L)*}$ Optimized results of uncertain variables in inner-master problem (MP)

$\boldsymbol{d}^{(q)*}$ Identified uncertain parameters in sub-problem (SP)

F_{m1}^{1}, F_{m1}^{2} The minimum on and off time limit coefficients of units

$f^{AC,\min}$, $f^{AC,\max}$, $P^{AC,\min}$, $P^{AC,\max}$ Operation frequencies and power limits of AC

k^P, μ^P, k^Q, μ^Q Constant coefficients of AC

$P_{p,t}^{AVES,ch,\max}$, $P_{p,t}^{AVES,dis,\max}$ Charging and discharging power limits of AVESs

$P_t^{AC,base}$, $Q_t^{AC,base}$ Operation power and cooling capacity baselines of AC

$P_{b1,t}^{D,e}$, $P_{b2,t}^{D,e}$ Predicted active power demands

$P_{b1,t}^{D,f}$, $P_{b2,t}^{D,f}$ Deviations of predicted active power demands

$P_d^{\min}$, $P_d^{\max}$ Lower and upper limits of boundary power

$P_{l1}^{\max}$, $P_{l2}^{\max}$, $Q_{l2}^{\max}$ Active and reactive power flow limits of lines

$P_{m1}^{G,\min}$, $P_{m2}^{G,\min}$, $P_{m1}^{G,\max}$, $P_{m2}^{G,\max}$ Lower and upper power output limits of units

$P_{m1}^{G,up,\max}$, $P_{m2}^{G,up,\max}$, $P_{m1}^{G,dn,\max}$, $P_{m2}^{G,dn,\max}$ Upward and downward ramping limits of units

$P_{w1,t}^{wind,e}$, $P_{w2,t}^{wind,e}$ Predicted wind power outputs

$P_{w1,t}^{wind,f}$, $P_{w2,t}^{wind,f}$ Deviations of predicted wind power outputs

$Q_{b2,t}^{D}$ Reactive power demands

$Q_{d,t}^{D}$ Reactive power supplied by substations

Q_t^{diss} Heat dissipation from people and appliances

$R_{m1}^{G,up,\max}$, $R_{m2}^{G,up,\max}$, $R_{m1}^{G,dn,\max}$, $R_{m2}^{G,dn,\max}$ Up- and down-spinning reserve limits of units

r_{l2}, x_{l1}, x_{l2} Resistances and reactances of lines

T Number of time intervals

$T^{\min}$, $T^{\max}$ Lower and upper limits of room temperature

T_t^{out} Ambient temperature

$T_{m1}^{on,\min}$, $T_{m1}^{off,\min}$ The minimum on and off time limits of units

T_{m1}^{on0}, T_{m1}^{off0} Cumulation on and off time of units

T^{set} Room temperature setpoint of AC

$V_{b2}^{\max}$ Phase magnitude limit of nodes

χ Constant coefficient greater than 1

$\boldsymbol{x}^{(Q)*}$ Optimized result of first-stage variables obtained by MP

$\boldsymbol{y}^{(q)*}$ Newly added recourse variable corresponding to $\boldsymbol{d}^{(q)*}$

$\boldsymbol{z}^{(l)*}$ Identified binary variables in inner-SP

D. Variables

η, θ Auxiliary variables in compact model

$\theta_{b1,t}$, $\theta_{b2,t}$ Phase angles of nodes

$\lambda_{d,t}^{P}$, $\lambda_{d,t}^{R\pm}$ Once multiplier of Lagrangian penalty function

ω^P, $\omega^{R\pm}$ Twice multipliers of Lagrangian penalty function

$AVSOC_{p,t}$, $vsoc_t$ SOC levels of AVESs and VES

$AVSOC_{p,t}^{\min}$, $AVSOC_{p,t}^{\max}$ The minimum and maximum SOC levels of AVESs

C^0 Operation cost in normal state

f_t^{AC} Compressor operation frequency of AC

$f_{d,t}^{+}$, $f_{d,t}^{-}$ Binary variables that reflect uncertain equivalent loads of DS

$f_{b1,t}^{D,+}$, $f_{b1,t}^{D,-}$, $f_{b2,t}^{D,+}$, $f_{b2,t}^{D,-}$ Binary variables that reflect uncertain loads

$f_{w1,t}^{wind,+}$, $f_{w1,t}^{wind,-}$, $f_{w2,t}^{wind,+}$, $f_{w2,t}^{wind,-}$ Binary variables that reflect uncertain wind power outputs

$P_{b1,t}^{D,curt}$, $P_{b2,t}^{D,curt}$ Load shedding quantities

$P_{w1,t}^{wind,curt}$, $P_{w2,t}^{wind,curt}$ Wind curtailment quantities

P_t^{AC}, Q_t^{AC} Operation power and cooling capacity of AC

$P_{p,t}^{AVES,ch}$, $P_{p,t}^{AVES,dis}$ Charging and discharging power of AVES

$P_{d,t}$ Boundary power

$P_{l1,t}$, $P_{l2,t}$, $Q_{l2,t}$ Active and reactive power of lines

$P_{m1,t}^{G}$, $P_{m2,t}^{G}$ Power outputs of units

$P_t^{VES,ch}$, $P_t^{VES,dis}$ Charging and discharging power of VES

$R_{d,t}^{+}$, $R_{d,t}^{-}$ Adjustable upward and downward boundary capacities

$R_{p,t}^{AVES,ch,up}$, $R_{p,t}^{AVES,ch,dn}$, $R_{p,t}^{AVES,dis,up}$, $R_{p,t}^{AVES,dis,dn}$	Upward and downward charging/discharging reserves of AVES
$R_{m1,t}^{G,up}$, $R_{m2,t}^{G,up}$, $R_{m1,t}^{G,dn}$, $R_{m2,t}^{G,dn}$	Upward and downward reserves of units
T_t^{in}	Indoor temperature of a room with AC
$u_{p,t}^{AVES}$	Binary variables that indicate charging/discharging states of AVESs (1 for discharging, 0 for charging)
$u_{m1,t}^{G}$, $u_{m2,t}^{G}$	Binary variables that indicate on and off states of units (1 for on, 0 for off)
$V_{b2,t}$	Voltage magnitude
$\boldsymbol{x}$, $\boldsymbol{z}$, $\boldsymbol{d}$	First-stage variables, second-stage binary variables, and uncertain variables

I. Introduction

THE increasing penetration of distributed energy resources has provided great opportunities and challenges to the operation of the transmission system (TS) and distribution systems (DSs) [1], [2]. On the one hand, the renewables and demand-side resources enable the traditional DSs to become active ones, which could supply power to local users and even to the TS [3]. On the other hand, the operation of TS and DSs suffers from an additional power supply-demand imbalance due to the intermittent outputs of renewables. In California, USA, it has been reported that a high penetration of renewables leads to significant difficulties for the operation of TS and DSs [4]. To accommodate the distributed energy resources economically and safely, the coordination between TS and DSs replaces the conventional separate management mode and is innovative in terms of fully exploiting the flexibility of the entire network.

Recent studies on the collaboration of TS and DSs include load restoration [5], economic dispatch [6], and optimal power flow [7]. In general, the coordinated operation can be implemented in a centralized [8] or distributed manner [5]-[7]. The centralized approaches require a control center to process the complete information of networks and solve the global optimization problem, which inevitably leads to high communication demands, complex large-scale optimization model formulations, and even privacy and cybersecurity issues. However, TS and DSs are managed independently by separate system operators. Therefore, adopting a centralized manner is impractical. By contrast, the distributed approaches provide an alternative to avoid the problems caused by centralized approaches. In a distributed manner, the integrated problem is divided into several subproblems by decomposition techniques such as the Benders decomposition approach [9], heterogeneous decomposition algorithm [6], multi-parametric programming [10], analytical target cascading (ATC) [5], and alternating direction approach of multipliers [11], [12].

Balancing supply and demand in real-time operations becomes more challenging as renewables with uncertain outputs increase in number. Thus, reserve allocation in distributed coordination has garnered wide attention, and different approaches such as chance-constrained programming [12], stochastic optimization [13], and robust optimization [14] have been introduced to handle uncertainties. A distributed coordination approach is proposed in [12] for the dynamic economic dispatch of TS and DSs, but the required reserve capacity for uncertainties is predetermined. In [15], a stochastic coordination model of TS and DSs is proposed to include renewable uncertainties, but the reserve schedule relies on numerous sampling scenarios or presupposed probability density functions. A coordinated operation scheme for TS and DSs is presented in [16] in which a robust optimization approach handles the uncertainties in renewables and loads. However, the aforementioned research works only consider the interaction of power between the TS and DSs, whereas the optimal reserve dispatch is restricted to the respective regional problem of each subsystem. The boundary power values are determined following optimization so that they cannot be flexibly regulated to match different requirements of the systems, which would result in lower renewable utilization, less operation flexibility, and poorer economic efficiency.

In addition, most studies related to TS and DS coordination have considered only the conventional generating units in the TS and distributed generators in the DSs, whereas the potential use of demand-side resources is also non-negligible. As a typical demand-side resource, air-conditioning loads have prominent advantages in demand response: ① air conditioners (ACs) account for a high proportion of the power demand, and the regulation potential is considerable; ② ACs possess the energy storage capacity and can be dispatched flexibly without compromising user comfort levels; ③ the peak electricity consumption period of air-conditioning loads is identical to that of the system peak load and, therefore, ACs can relieve the tension derived from the power supply-demand balance. In [17], thermostatically controlled loads such as ACs are investigated to provide an operation reserve for system reliability enhancement. Demand-side flexibility, including that of ACs, is exploited in [18] to maintain system security and operation economy. However, the focus of previous studies is either on the power shift or reserve supply, and none of them explore the energy and reserve co-dispatch of ACs. Apart from regular ACs with fixed frequencies, the potential of inverter ACs that account for approximately 30% of urban power consumption cannot be neglected [19]. Nevertheless, few studies have considered the effects of inverter ACs on the integrated TS and DS problem, and studies on user privacy protection are also scarce.

Motivated by the shortcomings of the existing research work, this paper presents a distributed and coordinated dispatch scheme for TS and active DSs to improve renewable utilization and system efficiency. The main contributions of this paper are as follows.

1) A distributed coordination framework is developed for the TS and active DSs, where two types of coupling variables, namely, active power and reserve capacity, are exchanged for interregional sharing of energy and reserve. Unlike existing research works [12], [15], [16], of which the fo-

cus is on power exchange, this paper also considers the sharing of upward and downward reserves. The boundary interactions are expanded from points to lines, and feasible access regions at the boundaries are then formed to cope with different system operation situations.

2) The ability of air-conditioning loads to enhance operation flexibility and provide reserves is investigated. The existing studies have rarely focused on inverter ACs. However, most current AC control is at the expense of user privacy violations. By contrast, the proposed aggregated virtual energy storage (AVES) model integrates decentralized inverter ACs to avoid these problems. In addition, compared with the existing studies on ACs that address only the power shift or reserve supply [17], [18], the energy and reserve co-dispatch of ACs is also explored in this paper. A reserve model of an AVES is constructed to incorporate air-conditioning resources into the optimal dispatch, where the flexibility of AVES is further activated by charging- or discharging-state elasticity.

3) A robust TS and DS coordination approach is proposed for jointly scheduling energy and reserves in a distributed manner, where the uncertainties of renewables and loads are considered. The resources on the supply and demand sides are fully utilized so that the independent subsystems can work cooperatively for the economic and efficiency enhancements. Given the non-convexity of the proposed TS and DS model derived from binary variables, a two-layer ATC algorithm is adopted to improve convergence.

The remainder of the paper is organized as follows. Section II describes the modeling of ACs. Sections III and IV present distributed coordination framework of TS and active DSs and detailed robust operation model of TS and DSs, respectively. Section V provides the solution methodology. Section VI presents case study, and Section VII draws the conclusion.

II. Modeling of ACs

A. Model of a Single AC

The equivalent thermal parameter model [20] is used to show the thermal dynamic process that occurs in a room, which can be expressed as:

$$C(\mathrm{d}T_t^{in}/\mathrm{d}t)=(T_t^{out}-T_t^{in})/R+Q_t^{diss}-Q_t^{AC} \tag{1}$$

The cooling capacity and operation power of the inverter AC can be adjusted by varying the operation frequency.

$$Q_t^{AC}=k^Q f_t^{AC}+\mu^Q \tag{2}$$

$$P_t^{AC}=k^P f_t^{AC}+\mu^P \tag{3}$$

$$f^{AC,\min}\le f_t^{AC}\le f^{AC,\max} \tag{4}$$

Considering the heat storage capacity of the inverter AC, a virtual energy storage (VES) model can be established to describe the operation conditions. If no external control signals exist, the AC will operate at the temperature setpoint under the cooling capacity and operation power baselines.

$$Q_t^{AC,base}=(T_t^{out}-T^{set})/R+Q_t^{diss} \tag{5}$$

$$P_t^{AC,base}=k^P[(T_t^{out}-T^{set})/R+Q_t^{diss}]/k^Q+(k^Q\mu^P-k^P\mu^Q)/k^Q \tag{6}$$

When external control signals are presented, the operation power of the AC can deviate from the baseline. Thus, the charging and discharging power of the VES can be described by:

$$P_t^{VES,ch}=P_t^{AC}-P_t^{AC,base}\quad P_t^{AC}\ge P_t^{AC,base} \tag{7}$$

$$P_t^{VES,dis}=P_t^{AC,base}-P_t^{AC}\quad P_t^{AC}<P_t^{AC,base} \tag{8}$$

$$0\le P_t^{VES,ch}\le P^{AC,\max}-P_t^{AC,base} \tag{9}$$

$$0\le P_t^{VES,dis}\le P_t^{AC,base}-P^{AC,\min} \tag{10}$$

The state of charge (SOC) of VES is the maximum or minimum when the room temperature reaches $T^{\min}$ or $T^{\max}$. Therefore, the SOC of VES is defined as:

$$vsoc_t=(T^{\max}-T_t^{in})/(T^{\max}-T^{\min}) \tag{11}$$

$$0\le vsoc_t\le 1 \tag{12}$$

From (1), (5)-(8), and (11), the variation at SOC level of VES is derived as:

$$vsoc_t=a\cdot vsoc_{t-1}+b(P_t^{VES,ch}-P_t^{VES,dis})+c \tag{13}$$

$$\begin{cases} a=\mathrm{e}^{-\Delta t/(RC)} \\ b=k^Q R(1-\mathrm{e}^{-\Delta t/(RC)})/[k^P(T^{\max}-T^{\min})] \\ c=(1-\mathrm{e}^{-\Delta t/(RC)})(T^{\max}-T^{set})/(T^{\max}-T^{\min}) \end{cases} \tag{14}$$

B. Model of Aggregated ACs

The energy-level evolution of an AC population can be obtained through a summation.

$$\sum_{i\in\mathcal{N}_p}\frac{vsoc_{i,t}}{b_i}=\sum_{i\in\mathcal{N}_p}\frac{a_i\cdot vsoc_{i,t-1}}{b_i}+\sum_{i\in\mathcal{N}_p}(P_{i,t}^{VES,ch}-P_{i,t}^{VES,dis})+\sum_{i\in\mathcal{N}_p}\frac{c_i}{b_i} \tag{15}$$

The SOC level and the charging and discharging power of the inverter AC population p are defined as:

$$AVSOC_{p,t}=\sum_{i\in\mathcal{N}_p}vsoc_{i,t}/b_i \tag{16}$$

$$P_{p,t}^{AVES,ch}=\sum_{i\in\mathcal{N}_p}P_{i,t}^{VES,ch} \tag{17}$$

$$P_{p,t}^{AVES,dis}=\sum_{i\in\mathcal{N}_p}P_{i,t}^{VES,dis} \tag{18}$$

The AVES model can then be given as:

$$AVSOC_{p,t}=A_p^A\cdot AVSOC_{p,t-1}+P_{p,t}^{AVES,ch}-P_{p,t}^{AVES,dis}+C_p^A \tag{19}$$

$$\begin{cases} A_p^A=\sum_{i\in\mathcal{N}_p}a_i/n_p \\ C_p^A=\sum_{i\in\mathcal{N}_p}c_{i,t}/b_i \end{cases} \tag{20}$$

$$0\le P_t^{AVES,ch}\le P_{p,t}^{AVES,ch,\max}=\sum_{i\in\mathcal{N}_p}(P_i^{AC,\max}-P_{i,t}^{AC,base}) \tag{21}$$

$$0\le P_t^{AVES,dis}\le P_{p,t}^{AVES,dis,\max}=\sum_{i\in\mathcal{N}_p}(P_{i,t}^{AC,base}-P_i^{AC,\min}) \tag{22}$$

$$0\le AVSOC_{p,t}\le AVSOC_{p,t}^{\mathrm{MAX}}=\sum_{i\in\mathcal{N}_p}1/b_i \tag{23}$$

Note that the average value is used to represent the heterogeneous a_i values in (20) for simplicity. Based on the AVES model, the aggregated ACs can be regulated just as in conventional energy storage, and ACs can be fully utilized without exposing users' private information.

III. Distributed Coordination Framework of TS and Active DSs

A typical network contains a single TS and multiple active DSs. The TS consists of conventional generators, renewable energy sources, passive loads directly connected, and active DS loads. Active DSs include distributed generators, renewable energy, nonflexible loads, and flexible loads.

The integration of distributed energy resources, including renewable energy sources and demand-side resources, enables the DS to transit from passive to active. In addition, the flexibility of active DSs is non-negligible for the collaborations between different subsystems. In general, the coordinated operation of TS and DSs can be realized in a centralized or distributed manner, which avoids the disadvantages of non-coordinated approaches such as boundary power mismatches and suboptimal dispatch schemes. However, when centralization problems such as computation and communication burdens as well as privacy violations are considered, coordinating the TS and DSs in a distributed manner is more appropriate.

The key to obtaining a distributed coordination of TS and DSs is to identify the proper boundary coupling variables between different systems. A distributed coordination framework of TS and DSs is presented in Fig. 1.

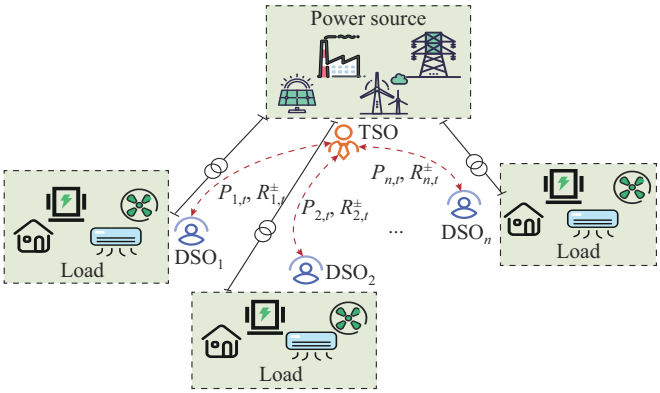

Fig. 1. Distributed coordination framework of TS and DSs.

Two types of boundary coupling variables, namely, active power $P_{d,t}$ and reserve capacity $R^{\pm}_{d,t}$, are exchanged to produce feasible access regions $[P_{d,t}-R^{-}_{d,t}, P_{d,t}+R^{+}_{d,t}]$ at the boundaries. These regions can adapt to the power supply-demand balance requirements under normal and uncertain conditions. The corresponding consistency constraints are given as:

$$P^{TS}_{d,t}=P^{DS}_{d,t} \tag{24}$$

$$R^{TS,+}_{d,t}=R^{DS,+}_{d,t} \tag{25}$$

$$R^{TS,-}_{d,t}=R^{DS,-}_{d,t} \tag{26}$$

IV. Robust Operation Model of TS and DSs

With the exchange of boundary information, the TS and DSs can operate independently under the uncertainties of renewable energy sources and load demands.

A. Mathematical Modeling of Robust Optimal Dispatch in TS

The objective function of TS in (27) is to minimize the total cost, which consists of two parts: the operation cost in the normal state and power imbalance cost in the uncertainty state.

$$\min C^{TS,0}+\max \min C^{TS,u} \tag{27}$$

The first part of the objective function and the corresponding constraints are given as:

$$\begin{aligned}\min C^{TS,0}=&\min_{\left(u^{TS,G}_{m1,t},P^{TS,G}_{m1,t},R^{TS,G,up}_{m1,t},R^{TS,G,dn}_{m1,t},\theta^{TS}_{bl,t},P^{TS}_{ll,t},P^{TS}_{d,t},R^{TS,+}_{d,t},R^{TS,-}_{d,t}\right)}\sum_{m_1\in\mathcal{G}^{TS}}\sum_{t\in\mathcal{T}}[C^{TS,SU}_{m1}\cdot\\&u^{TS,G}_{m1,t}(1-u^{TS,G}_{m1,t-1})+C^{TS,SD}_{m1}u^{TS,G}_{m1,t-1}(1-u^{TS,G}_{m1,t})+\\&\alpha^{TS,G}_{m1}(P^{TS,G}_{m1,t})^2+\beta^{TS,G}_{m1}P^{TS,G}_{m1,t}+\gamma^{TS,G}_{m1}u^{TS,G}_{m1,t}+C^{TS,G,up}_{m1}R^{TS,G,up}_{m1,t}+\\&C^{TS,G,dn}_{m1}R^{TS,G,dn}_{m1,t}]\end{aligned} \tag{28}$$

s.t.

$$\begin{cases}\sum_{t=1}^{F^1_{m1}}(1-u^{TS,G}_{m1,t})=0\\ F^1_{m1}=\max\{0,T^{on,\min}_{m1}-T^{on0}_{m1}\}\\ \sum_{\tau=t}^{t+T^{on,\min}_{m1}-1}u^{TS,G}_{m1,\tau}\ge T^{on,\min}_{m1}(u^{TS,G}_{m1,t}-u^{TS,G}_{m1,t-1})\\ \qquad t\in F^2_{m1}+1,F^2_{m1}+2,\ldots,T-T^{on,\min}_{m1}+1\\ \sum_{\tau=t}^{T}[u^{TS,G}_{m1,\tau}-(u^{TS,G}_{m1,t}-u^{TS,G}_{m1,t-1})]\ge 0\\ \qquad t\in T-T^{on,\min}_{m1}+2,T-T^{on,\min}_{m1}+3,\ldots,T\end{cases} \tag{29}$$

$$\begin{cases}\sum_{t=1}^{F^2_{m1}}u^{TS,G}_{m1,t}=0\\ F^2_{m1}=\max\{0,T^{off,\min}_{m1}-T^{off0}_{m1}\}\\ \sum_{\tau=t}^{t+T^{off,\min}_{m1}-1}(1-u^{TS,G}_{m1,\tau})\ge T^{off,\min}_{m1}(u^{TS,G}_{m1,t-1}-u^{TS,G}_{m1,t})\\ \qquad t\in F^2_{m1}+1,F^2_{m1}+2,\ldots,T-T^{off,\min}_{m1}+1\\ \sum_{\tau=t}^{T}[(1-u^{TS,G}_{m1,\tau})-(u^{TS,G}_{m1,t-1}-u^{TS,G}_{m1,t})]\ge 0\\ \qquad t\in T-T^{off,\min}_{m1}+2,T-T^{off,\min}_{m1}+3,\ldots,T\end{cases} \tag{30}$$

$$u^{TS,G}_{m1,t}P^{TS,G,\min}_{m1}\le P^{TS,G}_{m1,t}\le u^{TS,G}_{m1,t}P^{TS,G,\max}_{m1} \tag{31}$$

$$P^{TS,G}_{m1,t}+R^{TS,G,up}_{m1,t}-(P^{TS,G}_{m1,t-1}-R^{TS,G,dn}_{m1,t-1})\le P^{TS,G,up,\max}_{m1} \tag{32}$$

$$P^{TS,G}_{m1,t}-R^{TS,G,dn}_{m1,t}-(P^{TS,G}_{m1,t-1}+R^{TS,G,up}_{m1,t-1})\ge -P^{TS,G,dn,\max}_{m1} \tag{33}$$

$$P^{TS,G}_{m1,t}+R^{TS,G,up}_{m1,t}\le u^{TS,G}_{m1,t}P^{TS,G,\max}_{m1} \tag{34}$$

$$P^{TS,G}_{m1,t}-R^{TS,G,dn}_{m1,t}\ge u^{TS,G}_{m1,t}P^{TS,G,\min}_{m1} \tag{35}$$

$$0\le R^{TS,G,up}_{m1,t}\le R^{TS,G,up,\max}_{m1} \tag{36}$$

$$0\le R^{TS,G,dn}_{m1,t}\le R^{TS,G,dn,\max}_{m1} \tag{37}$$

$$P^{TS}_{d,t}+R^{TS,+}_{d,t}\le P^{\max}_{d} \tag{38}$$

$$P_{d,t}^{TS}-R_{d,t}^{TS,-}\geq P_{d}^{\min} \tag{39}$$

$$\sum_{l_1\in\mathcal{L}^{TS}|to(l_1)=b_1}P_{l1,t}^{TS}-\sum_{l_1\in\mathcal{L}^{TS}|fr(l_1)=b_1}P_{l1,t}^{TS}=\sum_{m_1\in\mathcal{G}_{b1}^{TS}}P_{m1,t}^{TS,G}+\sum_{w_1\in\mathcal{W}_{b1}^{TS}}P_{w1,t}^{TS,wind,e}-P_{b1,t}^{TS,D,e}-\sum_{d\in\mathcal{B}_{b1}^{TS}}P_{d,t}^{TS} \tag{40}$$

$$-P_{l1}^{TS,\max}\leq P_{l1,t}^{TS}=(\theta_{fr(l1),t}^{TS}-\theta_{to(l1),t}^{TS})/x_{l1}^{TS}\leq P_{l1}^{TS,\max} \tag{41}$$

The first-part cost in (28) contains the start-up and shut-down cost, production cost, and reserve cost of the units. Constraints (29) and (30) define the minimum on and off time of the units, respectively. Constraints (31) and (35) limit the power outputs and ramping rates of units, and (36) and (37) give the reserve bounds of the units. Constraints (38) and (39) restrict the exchange power between TS and DSs at the boundaries, and (40) and (41) describe the power balance equations and power flow limits in the normal state, respectively.

The second part of the objective function and corresponding constraints are:

$$\min\max\min C^{TS,u}=\min\max_{f_{w1,t}^{TS,wind,+},f_{w1,t}^{TS,wind,-},f_{b1,t}^{TS,D,+},f_{b1,t}^{TS,D,-},f_{d,t}^{TS,+},f_{d,t}^{TS,-}}\min_{P_{w1,t}^{TS,wind,curt},P_{b1,t}^{TS,D,curt},\theta_{b1,t}^{TS,u},P_{l1,t}^{TS,u},P_{m1,t}^{TS,G,u}}\sum_{t\in\mathcal{T}}\sum_{w_1\in\mathcal{W}^{TS}}\left(C_{curt}^{wind}P_{w1,t}^{TS,wind,curt}+\sum_{t\in\mathcal{T}}\sum_{b_1\in\mathcal{B}^{TS}}C_{curt}^{D}P_{b1,t}^{TS,D,curt}\right) \tag{42}$$

s.t.

$$\sum_{l_1\in\mathcal{L}^{TS}|to(l_1)=b_1}P_{l1,t}^{TS,u}-\sum_{l_1\in\mathcal{L}^{TS}|fr(l_1)=b_1}P_{l1,t}^{TS,u}=\sum_{m_1\in\mathcal{G}_{b1}^{TS}}P_{m1,t}^{TS,G,u}-\sum_{d\in\mathcal{B}_{b1}^{TS}}P_{d,t}^{TS,u}+\sum_{w_1\in\mathcal{W}_{b1}^{TS}}(P_{w1,t}^{TS,wind,u}-P_{w1,t}^{TS,wind,curt})-(P_{b1,t}^{TS,D,u}-P_{b1,t}^{TS,D,curt}) \tag{43}$$

$$-P_{l1}^{TS,\max}\leq P_{l1,t}^{TS,u}=(\theta_{fr(l1),t}^{TS,u}-\theta_{to(l1),t}^{TS,u})/x_{l1}^{TS}\leq P_{l1}^{TS,\max} \tag{44}$$

$$P_{m1,t}^{TS,G}-R_{m1,t}^{TS,G,dn}\leq P_{m1,t}^{TS,G,u}\leq P_{m1,t}^{TS,G}+R_{m1,t}^{TS,G,up} \tag{45}$$

$$\begin{cases}P_{w1,t}^{TS,wind,u}=P_{w1,t}^{TS,wind,e}+P_{w1,t}^{TS,wind,f}(f_{w1,t}^{TS,wind,+}-f_{w1,t}^{TS,wind,-})\\ f_{w1,t}^{TS,wind,+}+f_{w1,t}^{TS,wind,-}\leq 1\\ \sum_{w_1\in\mathcal{W}^{TS}}(f_{w1,t}^{TS,wind,+}+f_{w1,t}^{TS,wind,-})\leq\Gamma^{TS,wind}\end{cases} \tag{46}$$

$$\begin{cases}P_{b1,t}^{TS,D,u}=P_{b1,t}^{TS,D,e}+P_{b1,t}^{TS,D,f}(f_{b1,t}^{TS,D,+}-f_{b1,t}^{TS,D,-})\\ f_{b1,t}^{TS,D,+}+f_{b1,t}^{TS,D,-}\leq 1\\ \sum_{b_1\in\mathcal{B}^{TS}}(f_{b1,t}^{TS,D,+}+f_{b1,t}^{TS,D,-})\leq\Gamma^{TS,D}\end{cases} \tag{47}$$

$$\begin{cases}P_{d,t}^{TS,u}=P_{d,t}^{TS}+R_{d,t}^{TS,+}f_{d,t}^{TS,+}-R_{d,t}^{TS,-}f_{d,t}^{TS,-}\\ f_{d,t}^{TS,+}+f_{d,t}^{TS,-}\leq 1\end{cases} \tag{48}$$

The second-part cost in (42) is the sum of the costs of load shedding and wind curtailment. Constraints (43) and (44) are the power balance equations and line flow limits for the uncertainty cases, respectively. Constraint (45) indicates that the outputs of the units can be re-dispatched according to the power and reserve contributions in the normal case. In addition, (46)-(48) construct uncertainty sets to describe the random wind power outputs, passive load demands of TS, and equivalent loads of DSs, respectively.

B. Mathematical Modeling of Robust Optimal Dispatch in DS

As a type of demand-side resource, air-conditioning loads are incorporated into the optimal dispatch of DSs. Similarly, the objective function of DS in (49) also minimizes the total cost.

$$\min C_{d}^{DS,0}+\max\min C_{d}^{DS,u} \tag{49}$$

The first part of the objective function and its constraints are expressed as:

$$\min C_{b}^{DS,0}=\min_{\substack{u_{m2,t}^{DS,G},P_{m2,t}^{DS,G},R_{m2,t}^{DS,G,up},R_{m2,t}^{DS,G,dn},P_{d,t}^{DS},R_{d,t}^{DS,+},R_{d,t}^{DS,-},P_{l2,t}^{DS},Q_{l2,t}^{DS},V_{b2,t}^{DS},u_{p,t}^{AVES},P_{p,t}^{AVES,ch},P_{p,t}^{AVES,dis},R_{p,t}^{AVES,ch,up},\\ R_{p,t}^{AVES,ch,dn},R_{p,t}^{AVES,dis,up},R_{p,t}^{AVES,dis,dn},AVSOC_{p,t},AVSOC_{p,t}^{\min},AVSOC_{p,t}^{\max}}}\left\{\sum_{m_2\in\mathcal{G}_{d}^{DS}}\sum_{t\in\mathcal{T}}[C_{m2}^{DS,SU}u_{m2,t}^{DS,G}(1-u_{m2,t-1}^{DS,G})+C_{m2}^{DS,SD}u_{m2,t-1}^{DS,G}(1-u_{m2,t}^{DS,G})+\right.$$
$$\alpha_{m2}^{DS,G}(P_{m2,t}^{DS,G})^2+\beta_{m2}^{DS,G}P_{m2,t}^{DS,G}+\gamma_{m2}^{DS,G}u_{m2,t}^{DS,G}+C_{m2}^{DS,G,up}R_{m2,t}^{DS,G,up}+C_{m2}^{DS,G,dn}R_{m2,t}^{DS,G,dn}]+\sum_{p\in\mathcal{VS}_d}\sum_{t\in\mathcal{T}}(C_{p}^{AVES,ch}P_{p,t}^{AVES,ch}+C_{p}^{AVES,dis}P_{p,t}^{AVES,dis}+$$
$$\left.C_{p}^{AVES,ch,up}R_{p,t}^{AVES,ch,up}+C_{p}^{AVES,ch,dn}R_{p,t}^{AVES,ch,dn}+C_{p}^{AVES,dis,up}R_{p,t}^{AVES,dis,up}+C_{p}^{AVES,dis,dn}R_{p,t}^{AVES,dis,dn})\right\} \tag{50}$$

s.t.

$$P_{d,t}^{DS}+R_{d,t}^{DS,+}\leq P_{d}^{\max} \tag{51}$$

$$P_{d,t}^{DS}-R_{d,t}^{DS,-}\geq P_{d}^{\min} \tag{52}$$

$$0\leq P_{p,t}^{AVES,ch}\leq P_{p,t}^{AVES,ch,\max}(1-u_{p,t}^{AVES}) \tag{53}$$

$$0\leq P_{p,t}^{AVES,dis}\leq P_{p,t}^{AVES,dis,\max}u_{p,t}^{AVES} \tag{54}$$

$$AVSOC_{p,t}=A_{p}^{A}\cdot AVSOC_{p,t-1}+P_{p,t}^{AVES,ch}-P_{p,t}^{AVES,dis}+C_{p}^{A} \tag{55}$$

$$0\leq P_{p,t}^{AVES,dis}+R_{p,t}^{AVES,dis,up}\leq P_{p,t}^{AVES,dis,\max} \tag{56}$$

$$0\leq P_{p,t}^{AVES,dis}-R_{p,t}^{AVES,dis,dn}\leq P_{p,t}^{AVES,dis,\max} \tag{57}$$

$$0\leq P_{p,t}^{AVES,ch}+R_{p,t}^{AVES,ch,dn}\leq P_{p}^{AVES,ch,\max} \tag{58}$$

$$0\leq P_{p,t}^{AVES,ch}+R_{p,t}^{AVES,ch,dn}\leq P_{p}^{AVES,ch,\max} \tag{59}$$

$$0\leq AVSOC_{p,t}^{\min}\leq AVSOC_{p,t}^{\max}\leq AVSOC_{p,t}^{\mathrm{MAX}} \tag{60}$$

$$AVSOC_{p,t}^{\min}\leq AVSOC_{p,t}\leq AVSOC_{p,t}^{\max} \tag{61}$$

$$AVSOC_{p,t}^{\min}\leq A_{p}^{A}\cdot AVSOC_{p,t-1}^{\min}-(P_{p,t}^{AVES,dis}+R_{p,t}^{AVES,dis,up})+(P_{p,t}^{AVES,ch}-R_{p,t}^{AVES,ch,up})+C_{p}^{A} \tag{62}$$

$$AVSOC_{p,t}^{\max}\geq A_{p}^{A}\cdot AVSOC_{p,t-1}^{\max}-(P_{p,t}^{AVES,dis}-R_{p,t}^{AVES,dis,dn})+(P_{p,t}^{AVES,ch}+R_{p,t}^{AVES,ch,dn})+C_{p}^{A} \tag{63}$$

$$\sum_{l_2\in\mathcal{L}_{d}^{DS}|to(l_2)=b_2}P_{l2,t}^{DS}-\sum_{l_2\in\mathcal{L}_{d}^{DS}|fr(l_2)=b_2}P_{l2,t}^{DS}=\sum_{d\in\mathcal{B}_{d,b2}^{DS}}P_{d,t}^{DS}+\sum_{m_2\in\mathcal{G}_{d,b2}^{DS}}P_{m2,t}^{DS,G}+\sum_{w_2\in\mathcal{W}_{d,b2}^{DS}}P_{w2,t}^{DS,wind,e}+\sum_{p\in\mathcal{VS}_{d,b2}}(P_{p,t}^{AVES,dis}-P_{p,t}^{AVES,ch})-P_{b2,t}^{DS,D,e} \tag{64}$$

$$\sum_{l_2 \in \mathcal{L}_d^{DS} \mid to(l_2)=b_2} Q_{l2,t}^{DS} - \sum_{l_2 \in \mathcal{L}_d^{DS} \mid fr(l_2)=b_2} Q_{l2,t}^{DS} = \sum_{d \in \mathcal{B}_{d,b2}^{DS}} Q_{d,t}^{DS} - Q_{b2,t}^{DS,D} \tag{65}$$

$$V_{j2,t}^{DS} - V_{b2,t}^{DS} = P_{l2,t}^{DS} r_{l2}^{DS} + Q_{l2,t}^{DS} x_{l2}^{DS} \quad \forall fr(l_2)=j_2, to(l_2)=b_2 \tag{66}$$

$$-P_{l2}^{DS,\max} \le P_{l2,t}^{DS} \le P_{l2}^{DS,\max} \tag{67}$$

$$-Q_{l2}^{DS,\max} \le Q_{l2,t}^{DS} \le Q_{l2}^{DS,\max} \tag{68}$$

$$-V_{b2}^{DS,\max} \le V_{b2,t}^{DS} \le V_{b2}^{DS,\max} \tag{69}$$

The first-part cost in (50) consists of the energy and reserve costs of the units and AVESs. The unit operation constraints, including the on or off time, upper or lower power and reserve, and ramping up and down rates, which are similar to those in (31) and (37), are omitted here but actually function properly. Constraints (51) and (52) restrict the exchanged power to the boundary. Constraints (53) and (54) are the charging and discharging power limits of AVESs, respectively. Constraint (55) is the SOC variations of AVESs, as illustrated in Section II-B. Constraints (56)-(63) define the ranges of the reserve capacity provided by AVESs in terms of the limits of charging/discharging power and energy levels. Specifically, AVESs can supply four types of reserves: up-discharging, down-discharging, up-charging, and down-charging. Constraints (56)-(59) are the reserve bounds of AVESs as limited by the charging/discharging power, respectively. In addition, the restrictions on the reserve contributions of AVESs from the SOC levels cannot be ignored; that is, the possible power outputs of AVESs adjusted by the reserve should still be maintained within the limiting ranges of SOC level. Constraints (60) and (61) are the SOC level limits of AVESs, and (62) and (63) are the possible variations at SOC levels considering the charging/discharging power outputs, reserve contributions, and the previous SOC levels. Remarkably, the charging/discharging states of AVESs in the uncertainty case can be regulated flexibly, regardless of those in the normal case, which is called charging/discharging state elasticity. As a result, greater reserve capacities can be obtained, as shown in Fig. 2. Constraints (64)-(69) provide the power balance equations, power flow limits, and voltage magnitude limits in the normal case based on the linearized DistFlow model.

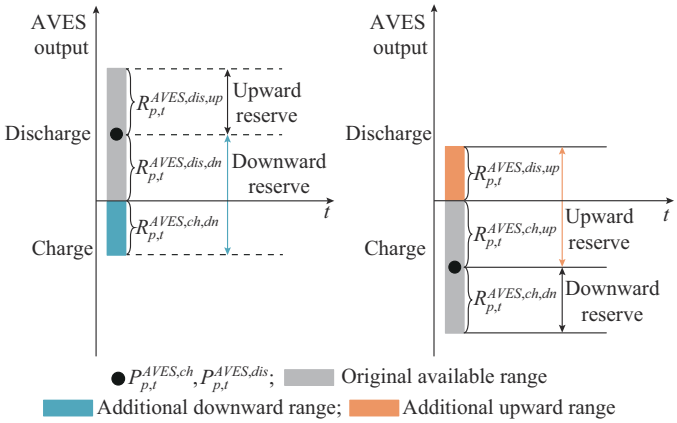

Fig. 2. Sketch of charging/discharging state elasticity.

The second part of the objective function and constraints are given as:

$$\min \max \min C_d^{DS,u} = \min \max_{f_{b2,t}^{DS,D,+}, f_{b2,t}^{DS,D,-}, f_{w2,t}^{DS,wind,+}, f_{w2,t}^{DS,wind,-}} \min_{\substack{P_{w2,t}^{DS,wind,curt}, P_{b2,t}^{DS,D,curt}, u_{p,t}^{AVES,u}, P_{p,t}^{AVES,ch,u}, \\ P_{p,t}^{AVES,dis,u}, P_{m2,t}^{DS,G,u}, P_{d,t}^{DS,u}, P_{l2,t}^{DS,u}, V_{b2,t}^{DS,u}}} \left\{ \sum_{t \in \mathcal{T}} \sum_{w_2 \in \mathcal{W}_d^{DS}} C_{curt}^{wind} P_{w2,t}^{DS,wind,curt} + \sum_{t \in \mathcal{T}} \sum_{b_2 \in \mathcal{B}_d^{DS}} C_{curt}^{D} P_{b2,t}^{DS,D,curt} \right\} \tag{70}$$

s.t.

$$\sum_{l_2 \in \mathcal{L}_d^{DS} \mid to(l_2)=b_2} P_{l2,t}^{DS,u} - \sum_{l_2 \in \mathcal{L}_d^{DS} \mid fr(l_2)=b_2} P_{l2,t}^{DS,u} = \sum_{m_2 \in \mathcal{G}_{d,b2}^{DS}} P_{m2,t}^{DS,G,u} + \sum_{d \in \mathcal{B}_{d,b2}^{DS}} P_{d,t}^{DS,u} + \sum_{p \in \mathcal{VS}_{d,b2}} (P_{p,t}^{AVES,dis,u} - P_{p,t}^{AVES,ch,u}) + \sum_{w_2 \in \mathcal{W}_{d,b2}^{DS}} (P_{w2,t}^{DS,wind,u} - P_{w2,t}^{DS,wind,curt}) - (P_{b2,t}^{DS,D,u} - P_{b2,t}^{DS,D,curt}) \tag{71}$$

$$V_{j2,t}^{DS,u} - V_{b2,t}^{DS,u} = P_{l2,t}^{DS,u} r_{l2}^{DS} + Q_{l2,t}^{DS} x_l^{DS} \quad \forall fr(l_2)=j_2, to(l_2)=b_2 \tag{72}$$

$$-P_{l2}^{DS,\max} \le P_{l2,t}^{DS,u} \le P_{l2}^{DS,\max} \tag{73}$$

$$-V_{b2}^{DS,\max} \le V_{b2,t}^{DS,u} \le V_{b2}^{DS,\max} \tag{74}$$

$$P_{m2,t}^{DS,G} - R_{m2,t}^{DS,G,dn} \le P_{m2,t}^{DS,G,u} \le P_{m2,t}^{DS,G} + R_{m2,t}^{DS,G,up} \tag{75}$$

$$0 \le P_{p,t}^{AVES,ch,u} \le P_{p,t}^{AVES,ch,\max}(1 - u_{p,t}^{AVES,u}) \tag{76}$$

$$0 \le P_{p,t}^{AVES,dis,u} \le P_{p,t}^{AVES,dis,\max} u_{p,t}^{AVES,u} \tag{77}$$

$$P_{p,t}^{AVES,ch} - R_{p,t}^{AVES,ch,up} \le P_{p,t}^{AVES,ch,u} \le P_{p,t}^{AVES,ch} + R_{p,t}^{AVES,ch,dn} \tag{78}$$

$$P_{p,t}^{AVES,dis} - R_{p,t}^{AVES,dis,dn} \le P_{p,t}^{AVES,dis,u} \le P_{p,t}^{AVES,dis} + R_{p,t}^{AVES,dis,up} \tag{79}$$

$$P_{d,t}^{DS} - R_{d,t}^{DS,-} \le P_{d,t}^{DS,u} \le P_{d,t}^{DS} + R_{d,t}^{DS,+} \tag{80}$$

$$\begin{cases} P_{w2,t}^{DS,wind,u} = P_{w2,t}^{DS,wind,e} + P_{w2,t}^{DS,wind,f}(f_{w2,t}^{DS,wind,+} - f_{w2,t}^{DS,wind,-}) \\ f_{w2,t}^{DS,wind,+} + f_{w2,t}^{DS,wind,-} \le 1 \\ \sum_{w_2 \in \mathcal{W}_d^{DS}} (f_{w2,t}^{DS,wind,+} + f_{w2,t}^{DS,wind,-}) \le \Gamma^{DS,wind} \end{cases} \tag{81}$$

$$\begin{cases} P_{b2,t}^{DS,D,u} = P_{b2,t}^{DS,D,e} + P_{b2,t}^{DS,D,f}(f_{b2,t}^{DS,D,+} - f_{b2,t}^{DS,D,-}) \\ f_{b2,t}^{DS,D,+} + f_{b2,t}^{DS,D,-} \le 1 \\ \sum_{b_2 \in \mathcal{B}_d^{DS}} (f_{b2,t}^{DS,D,+} + f_{b2,t}^{DS,D,-}) \le \Gamma_d^{DS,D} \end{cases} \tag{82}$$

The second-part cost in (70) is the sum of the load shedding and wind curtailment costs. Constraints (71)-(74) describe the power flow and voltage limits in the uncertainty case. The re-dispatch bounds of the units are given by (75). Constraints (76)-(79) set the re-dispatched output limits of AVESs based on the charging/discharging power and reserve contributions in the normal case. Constraint (80) is the exchange power bounds in the uncertainty case, and (81) and (82) are the constructed uncertainty sets of the wind power and DS loads, respectively.

V. Solution Methodology

A. Distributed Operation Based on a Two-layer ATC Algorithm

Based on the two-layer ATC algorithm, the integrated TS and DS problem can be decomposed into several subprob-

lems by relaxing the coupling constraints with augmented Lagrangian penalty functions. The regional objective functions are formulated as:

$$\min C^{TS,0}+\sum_{d\in\mathcal{B}^{con}}\sum_{t\in\mathcal{T}}[\lambda_{d,t}^{P}(P_{d,t}^{TS}-P_{d,t}^{DS})+\omega^{P}(P_{d,t}^{TS}-P_{d,t}^{DS})^2+\lambda_{d,t}^{R+}(R_{d,t}^{TS,+}-R_{d,t}^{DS,+})+\omega^{R+}(R_{d,t}^{TS,+}-R_{d,t}^{DS,+})^2+\lambda_{d,t}^{R-}(R_{d,t}^{TS,-}-R_{d,t}^{DS,-})+\omega^{R-}(R_{d,t}^{TS,-}-R_{d,t}^{DS,-})^2]+\max\min C^{TS,u} \tag{83}$$

$$\min C_{d}^{DS,0}+\sum_{t\in\mathcal{T}}[\lambda_{d,t}^{P}(P_{d,t}^{TS}-P_{d,t}^{DS})+\omega^{P}(P_{d,t}^{TS}-P_{d,t}^{DS})^2+\lambda_{d,t}^{R+}\cdot(R_{d,t}^{TS,+}-R_{d,t}^{DS,+})+\omega^{R+}(R_{d,t}^{TS,+}-R_{d,t}^{DS,+})^2+\lambda_{d,t}^{R-}(R_{d,t}^{TS,-}-R_{d,t}^{DS,-})+\omega^{R-}(R_{d,t}^{TS,-}-R_{d,t}^{DS,-})^2]+\max\min C_{d}^{DS,u} \tag{84}$$

The procedure for solving the distributed TS and DS problem using the standard ATC algorithm is shown in Algorithm 1.

Algorithm 1: standard ATC algorithm

1: Initialization. Set the initial values of coupling variables $P_{d,t}^{DS(0)}$, $R_{d,t}^{DS,\pm(0)}$, the Lagrangian multipliers $\lambda_{d,t}^{P(1)}$, $\lambda_{d,t}^{R\pm(1)}$, and the residual tolerance ε^r. Set the iteration index $k=1$.
2: **while do**
3: Solve the subproblem of TS, and $P_{d,t}^{TS(k)}$ and $R_{d,t}^{TS,\pm(k)}$ are obtained.
4: Solve the subproblem of each DS, and $P_{d,t}^{DS(k)}$ and $R_{d,t}^{DS,\pm(k)}$ are obtained.
5: Check the stop criteria. Calculate the residual:
$Res^{(k)}=\max\{\|P_{d,t}^{TS(k)}-P_{d,t}^{DS(k)}\|_2,\|R_{d,t}^{TS,+(k)}-R_{d,t}^{DS,+(k)}\|_2,\|R_{d,t}^{TS,-(k)}-R_{d,t}^{DS,-(k)}\|_2\}$
If $Res^{(k)}\le\varepsilon^r$, the procedure terminates.
6: Update the Lagrangian multipliers:
$\lambda_{d,t}^{P(k+1)}=\lambda_{d,t}^{P(k)}+2(\omega^{P(k)})^2(P_{d,t}^{TS(k)}-P_{d,t}^{DS(k)}),\omega^{P(k+1)}=\chi\omega^{P(k)}$
$\lambda_{d,t}^{R\pm(k+1)}=\lambda_{d,t}^{R\pm(k)}+2(\omega^{R\pm(k)})^2(R_{d,t}^{TS,R\pm(k)}-R_{d,t}^{DS,R\pm(k)}),\omega^{R\pm(k+1)}=\chi\omega^{R\pm(k)}$
7: Set $k=k+1$.
8: **end while**

However, the regional models of TS and DSs are nonconvex because of the binary variables, and the convergence of the standard ATC algorithm cannot be guaranteed. Thus, a two-layer ATC algorithm is adopted to enhance the performance, which is presented in Algorithm 2.

Algorithm 2: two-layer ATC algorithm

1: Initialization. Set the tolerance ε^C and the iteration index $s=1$. Relax the binary variables u^{TS}, u^{DS} of TS and DSs to continuous ones and solve the corresponding problem by ATC algorithm. The initial values of boundary variables $P_{d,t}^{(1)}$, $R_{d,t}^{\pm(1)}$ are obtained.
2: **while do**
3: Solve the subproblems of TS and DSs with the fixed $P_{d,t}^{(s)}$, $R_{d,t}^{\pm(s)}$, and the optimal solutions of binary variables $u^{TS(s)}$, $u^{DS(s)}$ as well as the corresponding total cost $C^{SUM(s)}$ are obtained.
4: Check the stop criteria. Calculate the residual of the total cost:
$ResC^{(s)}=\max\{|(C^{SUM(s)}-C^{SUM(s-1)})/C^{SUM(s)}|,|(C^{SUM(s-1)}-C^{SUM(s-2)})/C^{SUM(s-1)}|\}$
If $ResC^{k}\le\varepsilon^r$ && $u^{TS(s)}=u^{TS(s-1)}$ && $u^{DS(s)}=u^{DS(s-1)}$, terminate.
5: Solve the dispatch model of TS and DSs by ATC algorithm with fixed $u^{TS(s)}$, $u^{DS(s)}$, and the boundary variables $P_{d,t}^{(s+1)}$, $R_{d,t}^{\pm(s+1)}$ are obtained.
6: Set $s=s+1$.
7: **end while**

First, the subproblems of TS and DSs with the binary variables relaxed as continuous ones are solved by the standard ATC algorithm to obtain the initial values of the exchanged power and reserve at the boundaries. Then, according to the obtained boundary information, the regional models with fixed boundary power and reserve are solved separately, and the binary variables are optimized. The models with known binary variables are then solved by the standard ATC algorithm, and the interactive power and reserve at the boundaries are updated. The iteration process does not terminate until the stopping criteria are satisfied. The convergence of the two-layer ATC algorithm is presented in the Appendix A.

The two-layer ATC algorithm clearly improves the standard ATC algorithm in two respects for an overall performance improvement. One is to transform the original mixed-integer quadratic models into quadratic and mixed-integer linear programming models. The second is to reduce the number of variables and corresponding constraints.

B. C&CG Algorithm for Robust Optimization of Subsystems

A tri-level two-stage robust model for each subsystem is given in Section IV. As a typical approach for multilevel optimization problems, the conventional column-and-constraint generation (C&CG) algorithm [21] can be conveniently applied to the TS but not to DSs. The binary variables in the second stage of the DS models render strong duality theory invalid. Consequently, a nested C&CG algorithm is developed.

For convenience, the robust optimal dispatch model for each DS is formulated in a compact matrix form.

$$\min_{\boldsymbol{x}}\boldsymbol{A}^{\mathrm{T}}\boldsymbol{x}+\max_{\boldsymbol{d}\in\boldsymbol{D}}\min_{\boldsymbol{y},\boldsymbol{z}\in\boldsymbol{\Omega}(\boldsymbol{x},\boldsymbol{d})}(\boldsymbol{B}^{\mathrm{T}}\boldsymbol{y}+\boldsymbol{C}^{\mathrm{T}}\boldsymbol{z}) \tag{85}$$

s.t.

$$\boldsymbol{E}\boldsymbol{x}\le\boldsymbol{g} \tag{86}$$

$$\boldsymbol{\Omega}(\boldsymbol{x},\boldsymbol{d})=\{\boldsymbol{F}\boldsymbol{y}+\boldsymbol{G}\boldsymbol{z}\le\boldsymbol{f}-\boldsymbol{H}\boldsymbol{x}-\boldsymbol{J}\boldsymbol{d}\} \tag{87}$$

The model is decomposed into a master problem (MP) and a subproblem (SP) as follows, and the optimal solutions are obtained by iterative computation, as shown in Algorithm 3.

Algorithm 3: nested C&CG algorithm

1: Initialization. Set the lower bound $LB^O=-\infty$, the upper bound $UB^O=+\infty$, and the iteration index $Q=1$. Set the tolerance ε^O.
2: **while do**
3: Solve MP with given $\{\boldsymbol{d}^{(q)*},q=1,2,\ldots,Q-1\}$ to obtain $\boldsymbol{x}^{(Q)*}$ and $\eta^{(Q)*}$, and update $LB^O=\max\{LB^O,\boldsymbol{A}^{\mathrm{T}}\boldsymbol{x}^{(Q)*}+\eta^{(Q)*}\}$.
4: Solve SP with given $\boldsymbol{x}^{(Q)*}$ to obtain $y^{(Q)*}$, $z^{(Q)*}$, and $d^{(Q)*}$, and update $UB^O=\min\{UB^O,\boldsymbol{A}^{\mathrm{T}}\boldsymbol{x}^{(Q)*}+\boldsymbol{B}^{\mathrm{T}}\boldsymbol{y}^{(Q)*}+\boldsymbol{C}^{\mathrm{T}}\boldsymbol{z}^{(Q)*}\}$. The process is as follows.
1) Initialization. Set the lower bound $LB^I=-\infty$, the upper bound $LB^I=+\infty$, and the iteration index L=1. Set the tolerance ε^I.
while do
2) Solve inner-MP with given $\{\boldsymbol{z}^{(l)*},l=1,2,\ldots,L-1\}$ to obtain $\boldsymbol{d}^{(L)*}$ and $\theta^{(L)*}$, and update $LB^I=\max\{LB^I,\theta^{(L)*}\}$.
3) Solve inner-SP with given $\boldsymbol{d}^{(L)*}$ to obtain $\boldsymbol{y}^{(L)*}$and $\boldsymbol{z}^{(L)*}$, and update $UB^I=\min\{UB^I,\boldsymbol{B}^{\mathrm{T}}\boldsymbol{y}^{(L)*}+\boldsymbol{C}^{\mathrm{T}}\boldsymbol{z}^{(L)*}\}$.
4) Convergence check. If $UB^I-LB^I\le\varepsilon^I$, terminate and output results. Otherwise, set $L=L+1$.
end while
5: Convergence check. If $UB^O-LB^O\le\varepsilon^O$, return the optimal results and terminate the calculation. Otherwise, set $Q=Q+1$.
6: **end while**

1) MP

$$\min_{\boldsymbol{x},\eta}(\boldsymbol{A}^{\mathrm{T}}\boldsymbol{x}+\eta) \tag{88}$$

s.t.

$$\boldsymbol{E}\boldsymbol{x} \le \boldsymbol{g} \tag{89}$$

$$\eta \ge \boldsymbol{B}^{\mathrm{T}}\boldsymbol{y}^{(q)} + \boldsymbol{C}^{\mathrm{T}}\boldsymbol{z}^{(q)} \quad q = 1, 2, \ldots, Q-1 \tag{90}$$

$$\boldsymbol{F}\boldsymbol{y}^{(q)} + \boldsymbol{G}\boldsymbol{z}^{(q)} \le \boldsymbol{f} - \boldsymbol{H}\boldsymbol{x} - \boldsymbol{J}\boldsymbol{d}^{(q)*} \quad q = 1, 2, \ldots, Q-1 \tag{91}$$

2) SP

$$\max_{\boldsymbol{d} \in \boldsymbol{D}} \min_{\boldsymbol{y}, \boldsymbol{z}} (\boldsymbol{B}^{\mathrm{T}}\boldsymbol{y} + \boldsymbol{C}^{\mathrm{T}}\boldsymbol{z}) \tag{92}$$

s.t.

$$\boldsymbol{F}\boldsymbol{y} + \boldsymbol{G}\boldsymbol{z} \le \boldsymbol{f} - \boldsymbol{H}\boldsymbol{x}^{(Q)*} - \boldsymbol{J}\boldsymbol{d} \tag{93}$$

The problem is transformed into a tri-level problem with a structure similar to that of the conventional two-stage robust model, and both inner MP and inner SP are generated.

$$\text{Inner MP: } \max_{\boldsymbol{d}, \theta} \theta \tag{94}$$

s.t.

$$\theta \le \boldsymbol{C}^{\mathrm{T}}\boldsymbol{z}^{(l)*} + (\boldsymbol{\pi}^{(l)})^{\mathrm{T}}(\boldsymbol{H}\boldsymbol{x}^{(Q)*} - \boldsymbol{J}\boldsymbol{d} - \boldsymbol{G}\boldsymbol{z}^{(l)*} - \boldsymbol{f}) \quad l = 1, 2, \ldots, L-1 \tag{95}$$

$$(\boldsymbol{\pi}^{(l)})^{\mathrm{T}}\boldsymbol{F} + \boldsymbol{B}^{\mathrm{T}} = \boldsymbol{0} \quad l = 1, 2, \ldots, L-1 \tag{96}$$

$$\boldsymbol{\pi}^{(l)} \ge \boldsymbol{0} \quad l = 1, 2, \ldots, L-1 \tag{97}$$

$$\text{Inner SP: } \min_{\boldsymbol{y}, \boldsymbol{z}} (\boldsymbol{B}^{\mathrm{T}}\boldsymbol{y} + \boldsymbol{C}^{\mathrm{T}}\boldsymbol{z}) \tag{98}$$

s.t.

$$\boldsymbol{F}\boldsymbol{y} + \boldsymbol{G}\boldsymbol{z} \le \boldsymbol{f} - \boldsymbol{H}\boldsymbol{x}^{(Q)*} - \boldsymbol{J}\boldsymbol{d}^{(L)*} \tag{99}$$

VI. Case Studies

To validate the effectiveness of the proposed approach, the performances of three test systems (T6D2, T118D10, and T118D30) are analyzed. All case studies are conducted using CPLEX 12.9.0 on a PC with an Intel Core i7 2.80 GHz and 8 GB RAM.

A. Results of Studies on T6D2

The T6D2 test system [22] consists of a 6-bus TS and two connected active DSs (DS1 and DS2), and its topology is shown in Fig. 3. The installed capacities of the wind farms in the three subsystems are 150 MW, 10 MW, and 20 MW, respectively. TS, DS1, and DS2 contain 3, 2, and 2 generating units, respectively.

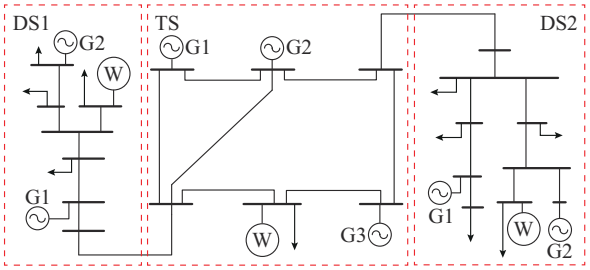

Fig. 3. Topology of T6D2.

1) Performance of Proposed Approach

The optimal dispatch results of TS and DSs are presented in Fig. 4.

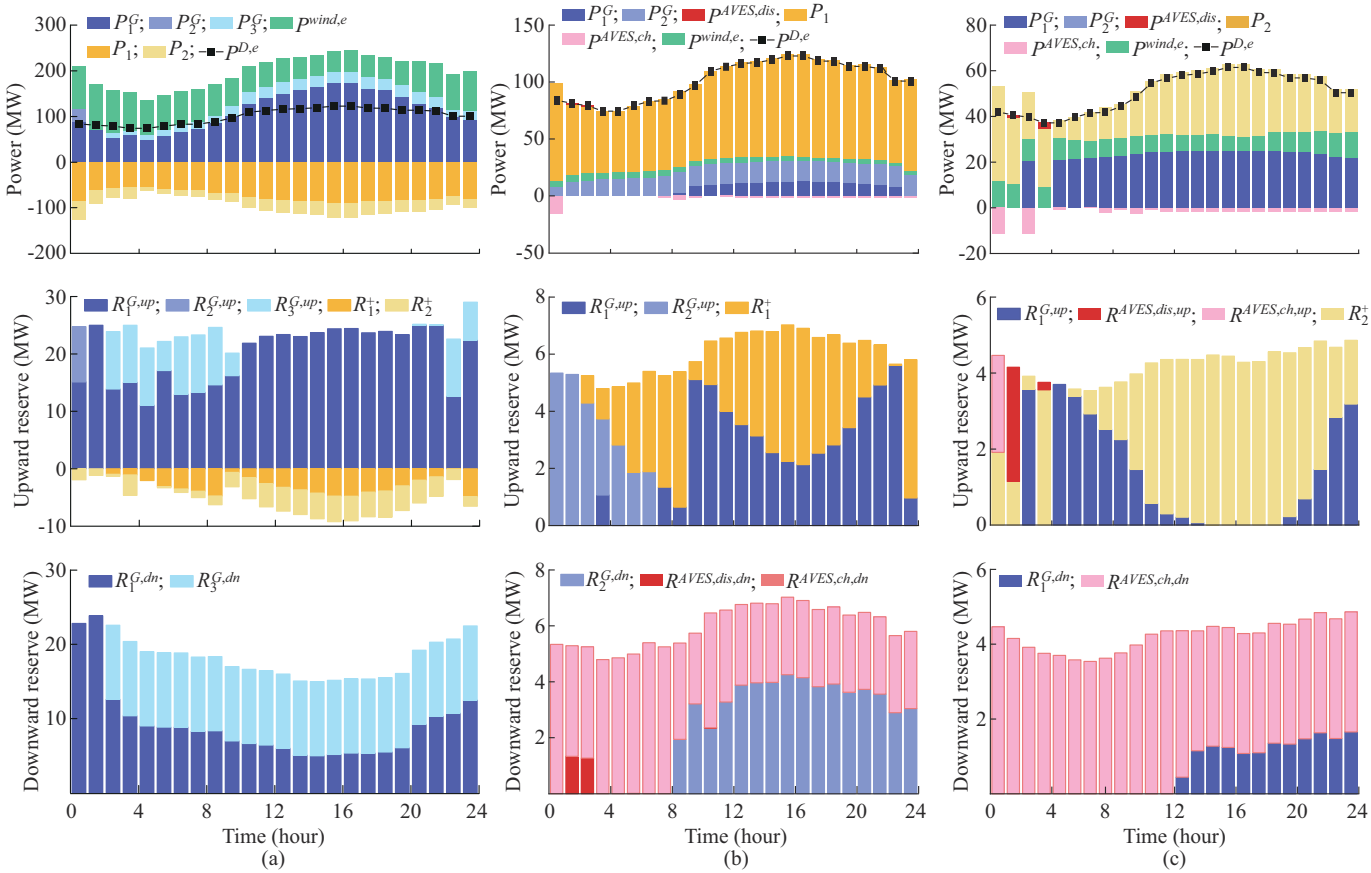

Fig. 4. Optimal dispatch results of TS and DSs. (a) TS. (b) DS1. (c) DS2.

It can be observed that the coordination between the TS and active DSs can be implemented by utilizing the flexibility of resources from different subsystems in a distributed and interactive manner. The energy and reserve contributions of the units, wind turbines, and air-conditioning loads are shared interregionally for the generation-load balance in different cases. Specifically, the power outputs of the generation resources in the TS are transmitted to DS1 and DS2 to satisfy the load demands in the normal case. In addition, the TS supplies part of the DS reserves to relieve the supply-demand pressure in the uncertainty cases.

Figure 4 also presents the flexibility of AVESs in the active DSs. First, AVESs perform power shifts by charging and discharging behaviors to avoid unnecessary load shedding or wind curtailment. For example, as shown in Fig. 4(b), the excessive wind power in DS1 during period 1 is absorbed by AVES instead of being abandoned. In addition, AVESs provide significant reserve support for DSs, as shown in Fig. 4(c), where most of the reserve capacity of DS2 is offered by the AVES. Moreover, the performance of the AVES during periods 2-3 as shown in Fig. 4(b) embodies its charging/discharging state elasticity.

Figure 5 shows a comparison of the boundary power between TS and DS2, where the installed capacity of the wind farm in DS2 is set to be 20 MW under low penetration or 100 MW under high penetration. The negative (positive) sign of boundary power means that TS (DS2) transmits power to DS2 (TS). It can be observed that DS2 can send power back to TS when the wind power is great, which illustrates the effects of renewables and demand-side resources on converting DSs from passive to active. Therefore, the flexibility of DSs can be utilized to improve their efficiency as well as those of the TS and DSs overall.

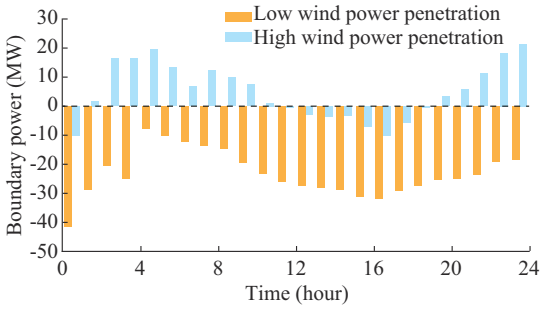

Fig. 5. Comparisons of boundary power between TS and DS2 with low and high wind power penetrations.

2) Impacts of AVESs on Active DSs

The virtual storage effectiveness of air-conditioning loads is illustrated by comparing the optimal results of cases with and without AVESs. The comparison results are listed in Table I and Fig. 6 shows that the exploitation of AVESs eliminates the power-imbalance cost and further reduces the total cost. Figure 6 presents the reserves of DSs with and without AVESs. The upward and downward reserve shortages during period 1 are compensated by the up- and down-charging reserves provided by AVESs, which effectively prevent load shedding and increase wind utilization.

TABLE I
RESULTS OF CASES WITH AND WITHOUT AVES

Scenario	TS			DS1			DS2			Total ($)
	Energy cost ($)	Reserve cost ($)	Power imbalance cost ($)	Energy cost ($)	Reserve cost ($)	Power imbalance cost ($)	Energy cost ($)	Reserve cost ($)	Power imbalance cost ($)	
With AVES	38801.22	6685.49	0.00	6217.65	456.71	0.0	6043.32	276.14	0.00	58480.53
Without AVES	37571.92	6518.10	3823.49	5956.06	530.61	931.8	6077.77	380.56	893.08	62683.40

3) Comparison with Other Approaches

The following three cases are studied to show the characteristics of the proposed approach, and comparison results are presented in Table II and Fig. 7.

1) Case 1: non-coordinated dispatch approach, where the boundary power is set as the predicted net load.

2) Case 2: conventional distributed dispatch approach, where only active power interaction is considered.

3) Case 3: the proposed distributed dispatch approach, where the reserve capacity interaction is also considered to form a feasible access region at the boundaries.

As Table II shows, compared with the non-coordinated approach in Case 1, more economical results, i.e., a lower total cost (at least a 20% decrease), can be obtained by the coordination of TS and DSs. In addition, the proposed approach (Case 3) can further reduce the total operation cost as compared with Case 2. This is because when energy and reserves are shared among different subsystems, more flexible resources with lower costs can be utilized to handle the uncertainties, resulting in improved economic performance.

Figure 7 compares the boundary power between TS and DSs in the three cases. The power exchanged at the boundaries in Cases 1 and 2 is deterministic and unchangeable. By contrast, the boundary power in Case 3 can be varied in the respective feasible access regions for uncertainty cases due to the interaction of the reserve capacity. Accordingly, the overuse or underuse of regional resources can be prevented, and the flexibility of TS and active DSs can be synthesized.

B. Results of Studies on T118D10

The T118D10 test system is composed of a modified IEEE 118-bus TS [23] and 10 modified IEEE 33-bus active DSs connected at buses 6, 7, 19, 20, 27, 28, 57, 70, 84, and 90. The same general results can be obtained when the proposed approach is compared with the conventional approach for T118D10. Figure 8 indicates that the proposed approach can further activate the flexibility of more dispatchable resources and consequently achieve more economical operation performance.

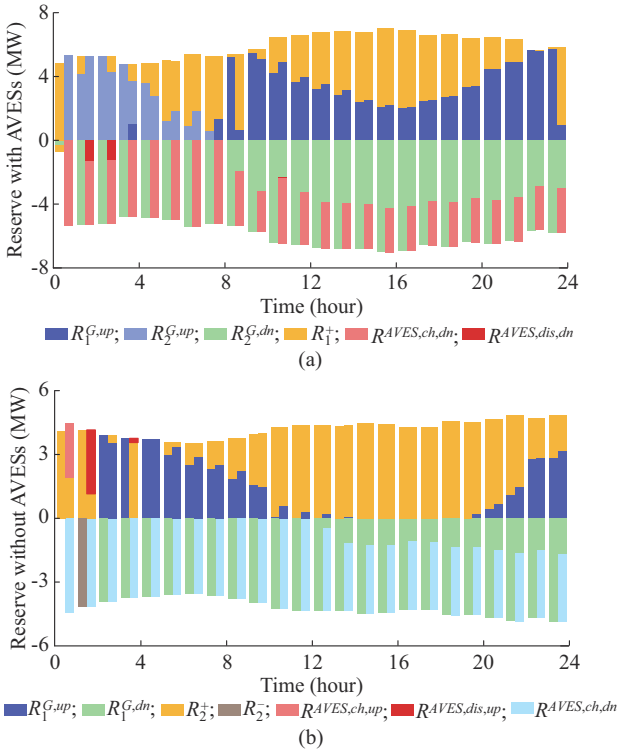

Fig. 6. Reserves of DSs with and without AVESs. (a) With AVESs for DS1. (b) Without AVESs for DS2.

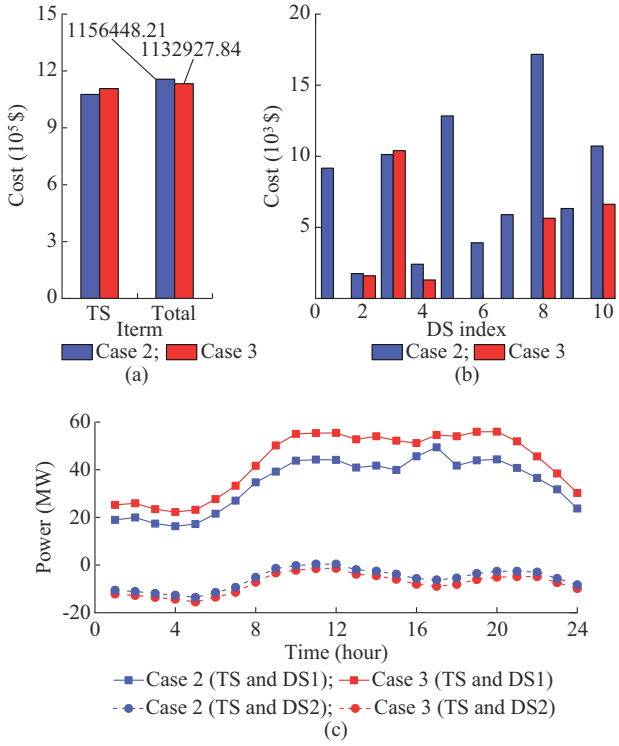

Fig. 8. Comparisons between Case 2 and Case 3 for T118D10. (a) TS and total costs. (b) Costs of DSs. (c) Boundary power.

TABLE II
OPEARTION COSTS OF DIFFERENT DISPATCH APPROACHES

Case	Cost ($)			
	TS	DS1	DS2	Total
Case 1	62386.85	7556.23	3417.08	73360.17
Case 2	45008.54	6784.25	6895.44	58688.23
Case 3	45486.71	6674.36	6319.46	58480.53

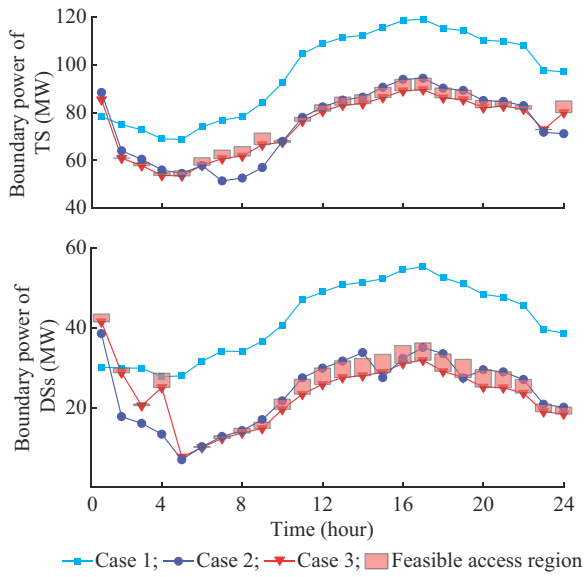

Fig. 7. Comparisons of boundary power between TS and DSs in three cases.

To validate the effectiveness of the two-layer ATC algorithm, the solution processes of the standard and two-layer ATC algorithms on the two test systems of T6D2 and T118D10 are compared in Fig. 9. The gap tolerances of power and reserve are set to be 0.1 MW and 0.01 MW, respectively. For the T6D2 test system, the two-layer ATC algorithm converges after three outer and 19 inner iterations, whereas the standard ATC algorithm converges after 24 iterations. Specifically, based on the two-layer ATC algorithm, the regional problems of the TS and DSs are solved with the binary variables relaxed as continuous variables at the first outer iteration, and the initial boundary variables of power and reserve are obtained. Next, with the fixed boundary variables, the TS, DS1, and DS2 are independently solved using the C&CG algorithm to obtain the binary variables. Then, the regional models with fixed binary variables are solved to obtain the updated boundary variables at another outer iteration. Finally, the entire solution procedure converges after several cycles. For the T118D10 test system, the two-layer ATC algorithm converges after three outer and 24 inner iterations. However, the maximum residuals of the standard ATC algorithm continue to oscillate, and the convergence fails within 50 iterations. Therefore, compared with the standard ATC algorithm, the two-layer ATC algorithm offers a stronger convergence property.

C. Results of Studies on T118D30

The proposed approach is also tested on a larger system, i.e., T118D30, including a modified IEEE 118-bus TS with 30 modified IEEE 33-bus active DSs.

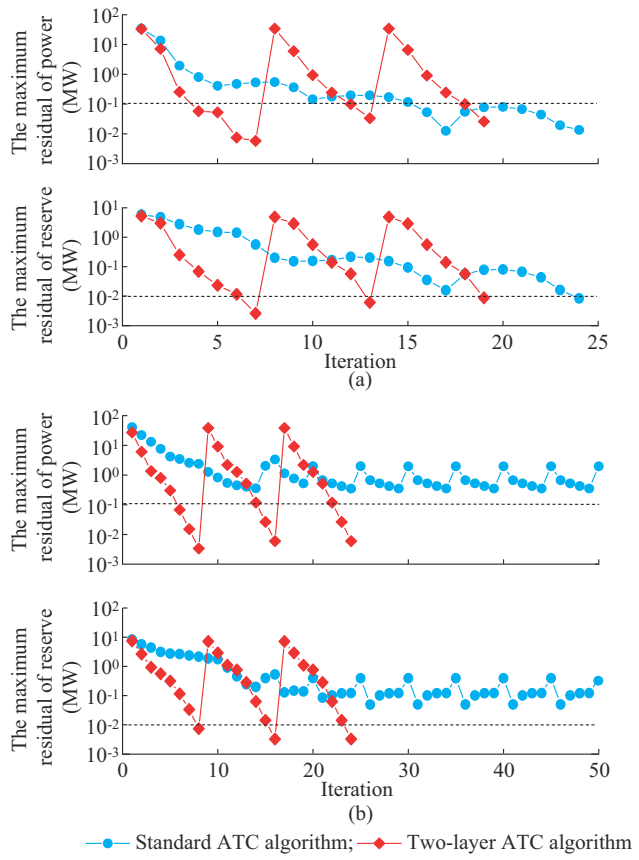

Fig. 9. Solution process of standard and two-layer ATC algorithms on two test systems. (a) T6D2. (b) T118D10.

The proposed approach is also compared with the conventional approach, and the cost results are shown in Table III. The results suggest that interregional energy and reserve support promote the efficient utilization of controllable resources in different systems, and a better dispatch approach with a lower operation cost is obtained by the proposed approach.

TABLE III
COST RESULTS OF T118D30

Case	TS			DS		
	Energy cost ($)	Reserve cost ($)	Subtotal ($)	Energy cost ($)	Reserve cost ($)	Subtotal ($)
2	1111623.62	95789.21	1207412.84	197339.21	58487.81	255827.02
3	1143040.80	126471.06	1269511.86	126632.15	24853.08	151485.24

Moreover, to demonstrate the effectiveness of the robust dispatch approach in handling uncertainties, out-of-sample simulations based on the Monte Carlo approach are conducted. Table IV summarizes the out-of-sample results under different budgets of TS wind uncertainty. The robust model clearly outperforms the deterministic model in terms of cost and power balance. The distributions of the power imbalance as depicted in Fig. 10 shows that the robust model with a larger uncertainty budget corresponds to a higher cost but better risk-coping performance. Thus, a trade-off between cost-effectiveness and risk aversion can be realized by appropriately adjusting the uncertainty budgets.

TABLE IV
OUT-OF-SAMPLE RESULTS UNDER DIFFERENT BUDGETS OF TS WIND UNCERTAINTY

Scenario	Cost ($)	Average power imbalance (MW)	The maximum power imbalance (MW)
Deterministic	1242762.59	3099.27	5539.70
$\Gamma^{TS,wind}=1$	1387582.64	33.35	748.14
$\Gamma^{TS,wind}=2$	1397707.69	19.97	659.72
$\Gamma^{TS,wind}=3$	1406673.48	12.68	587.02
$\Gamma^{TS,wind}=4$	1414216.80	8.67	529.58
$\Gamma^{TS,wind}=5$	1420997.10	6.27	477.75

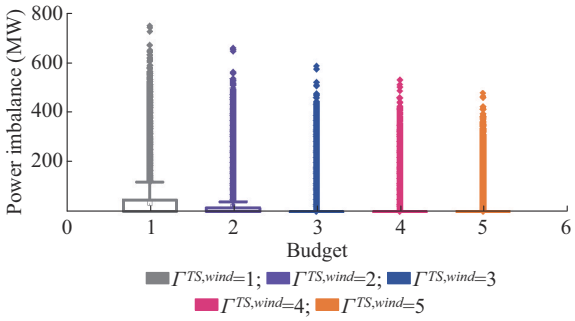

Fig. 10. Power imbalance distributions under different budgets of TS wind uncertainty in out-of-sample simulations.

VII. CONCLUSION

As the penetration of renewable energy sources increases, research efforts on the flexibility of active DSs and the interaction between the TS and DSs have also increased. To fully utilize dispatchable resources in active DSs and cope with the uncertainties of renewables and loads, this paper proposes a distributed robust coordination model of TS and DSs. In this model, the generating units and air-conditioning loads serve as flexible power and reserve supply resources, respectively. The coupling variables, i.e., active power and reserve capacity, are exchanged to share the feasible access boundary regions applicable to the normal and uncertainty cases. Accordingly, the communication and computation burdens are relieved and system privacy information is preserved. The two-layer ATC algorithm is combined with the nested C&CG algorithm to solve the optimization model in a distributed manner. Numerical results confirm that the proposed approach is superior to non-coordinated and conventional coordinated approaches in terms of economy and reliability.

APPENDIX A

The convergence of the two-layer ATC algorithm is proven as follows.

The coordination model of TS and DSs can be expressed in a concise format.

$$\begin{cases} \min F(\boldsymbol{u}, \boldsymbol{B}) \\ \text{s.t. } \boldsymbol{u} \in \Omega^{u} \\ \quad \boldsymbol{B} \in \Omega^{B} \end{cases} \tag{A1}$$

where $\boldsymbol{u}$ and $\boldsymbol{B}$ are the binary and boundary variables. According to the solving procedure stated in Section V-A, binary vari-

ables are first relaxed as continuous ones, and optimized objective function value, i.e., the lower bound of $F(\boldsymbol{u},\boldsymbol{B})$ is obtained.

At the s^{th} iteration, $F(\boldsymbol{u},\boldsymbol{B})$ is minimized with the fixed boundary variables $\boldsymbol{B}^{(s)}$, and the binary variables $\boldsymbol{u}^{(s)}$ are obtained.

$$\begin{cases} \boldsymbol{u}^{(s)} = \arg\min_{\boldsymbol{u}} F(\boldsymbol{u}, \boldsymbol{B}^{(s)}) \\ F(\boldsymbol{u}^{(s)}, \boldsymbol{B}^{(s)}) \le F(\boldsymbol{u}, \boldsymbol{B}^{(s)}) \end{cases} \tag{A2}$$

Then, $F(\boldsymbol{u},\boldsymbol{B})$ is minimized with the fixed binary variables $\boldsymbol{u}^{(s)}$, and the boundary variables $\boldsymbol{B}^{(s+1)}$ are obtained.

$$\begin{cases} \boldsymbol{B}^{(s+1)} = \arg\min_{\boldsymbol{B}} F(\boldsymbol{u}^{(s)}, \boldsymbol{B}) \\ F(\boldsymbol{u}^{(s)}, \boldsymbol{B}^{(s+1)}) \le F(\boldsymbol{u}^{(s)}, \boldsymbol{B}) \end{cases} \tag{A3}$$

Next, the iteration index goes to s+1, and $F(\boldsymbol{u},\boldsymbol{B})$ is minimized with the fixed boundary variables $\boldsymbol{B}^{(s+1)}$, and the binary variables $\boldsymbol{u}^{(s+1)}$ are obtained.

$$\begin{cases} \boldsymbol{u}^{(s+1)} = \arg\min_{\boldsymbol{u}} F(\boldsymbol{u}, \boldsymbol{B}^{(s+1)}) \\ F(\boldsymbol{u}^{(s+1)}, \boldsymbol{B}^{(s+1)}) \le F(\boldsymbol{u}, \boldsymbol{B}^{(s+1)}) \end{cases} \tag{A4}$$

Based on (A2)-(A4), (A5) can be derived as:

$$F(\boldsymbol{u}^{(s+1)}, \boldsymbol{B}^{(s+1)}) \le F(\boldsymbol{u}^{(s)}, \boldsymbol{B}^{(s+1)}) \le F(\boldsymbol{u}^{(s)}, \boldsymbol{B}^{(s)}) \tag{A5}$$

It can be observed that $F(\boldsymbol{u},\boldsymbol{B})$ is non-increasing during the iteration. Considering the known lower bound of $F(\boldsymbol{u},\boldsymbol{B})$, the convergence can be guaranteed.

REFERENCES

[1] M. Wang, Y. Wu, M. Yang *et al*., "Dynamic economic dispatch considering transmission-distribution coordination and automatic regulation effect," *IEEE Transactions on Industry Applications*, vol. 58, no. 3, pp. 3164-3174, May 2022.

[2] D. Shukla and S. P. Singh, "Aggregated effect of active distribution system on available transfer capability using multi-agent system based ITD framework," *IEEE Systems Journal*, vol. 15, no. 1, pp. 1401-1412, Mar. 2021.

[3] L. Tziovani, L. Hadjidemetriou, P. Kolios *et al*., "Energy management and control of photovoltaic and storage systems in active distribution grids," *IEEE Transactions on Power Systems*, vol. 37, no. 3, pp. 1956-1968, May 2022.

[4] A. Olson, A. Mahone, E. Hart *et al*., "Halfway there: can California achieve a 50% renewable grid?" *IEEE Power and Energy Magazine*, vol. 13, no. 4, pp. 41-52, Jul. 2015.

[5] J. Zhao, H. Wang, Q. Wu *et al*., "Optimal generator start-up sequence for bulk system restoration with active distribution networks," *IEEE Transactions on Power Systems*, vol. 36, no. 3, pp. 2046-2057, May 2021.

[6] Z. Li, Q. Guo, H. Sun *et al*., "A new LMP-sensitivity-based heterogeneous decomposition for transmission and distribution coordinated economic dispatch," *IEEE Transactions on Smart Grid*, vol. 9, no. 2, pp. 931-941, Mar. 2018.

[7] A. Nawaz and H. Wang, "Risk-aware distributed optimal power flow in coordinated transmission and distribution system," *Journal of Modern Power Systems and Clean Energy*, vol. 9, no. 3, pp. 502-515, May 2021.

[8] S. M. Mohseni-Bonab, I. Kamwa, A. Moeini *et al*., "Voltage security constrained stochastic programming model for day-ahead BESS schedule in co-optimization of T&D systems," *IEEE Transactions on Sustainable Energy*, vol. 11, no. 1, pp. 391-404, Jan. 2020.

[9] A. Rabiee and M. Parniani, "Voltage security constrained multi-period optimal reactive power flow using benders and optimality condition decompositions," *IEEE Transactions on Power Systems*, vol. 28, no. 2, pp. 696-708, May 2013.

[10] C. Lin, W. Wu, X. Chen *et al*., "Decentralized dynamic economic dispatch for integrated transmission and active distribution networks using multi-parametric programming," *IEEE Transactions on Smart Grid*, vol. 9, no. 5, pp. 4983-4993, Sept. 2018.

[11] P. Lan, G. Wu, X. Shen *et al*., "Distributed optimal scheduling for coupled transmission-distribution integrated electricity-gas system," *Electric Power Systems Research*, vol. 206, p. 107759, Feb. 2022.

[12] J. Zhai, Y. Jiang, Y. Shi *et al*., "Distributionally robust joint chance-constrained dispatch for integrated transmission-distribution systems via distributed optimization," *IEEE Transactions on Smart Grid*, vol. 13, no. 3, pp. 2132-2147, May 2022.

[13] J. Liu, H. Cheng, P. Zeng *et al*., "Decentralized stochastic optimization based planning of integrated transmission and distribution networks with distributed generation penetration," *Applied Energy*, vol. 220, pp. 800-813, Jun. 2018.

[14] Y. Ji, Q. Xu, J. Zhao *et al*., "Day-ahead and intra-day optimization for energy and reserve scheduling under wind uncertainty and generation outages," *Electric Power Systems Research*, vol. 195, p. 107133, Mar. 2021.

[15] A. Nawaz and H. Wang, "Distributed stochastic security constrained unit commitment for coordinated operation of transmission and distribution system," *CSEE Journal of Power and Energy Systems*, vol. 7, no. 4, pp. 708-718, Jul. 2021.

[16] M. K. Arpanahi, M. E. H. Golshan, and P. Siano, "A comprehensive and efficient decentralized framework for coordinated multiperiod economic dispatch of transmission and distribution Systems," *IEEE Systems Journal*, vol. 15, no. 2, pp. 2583-2594, Jun. 2021.

[17] Y. Ding, W. Cui, S. Zhang *et al*., "Multi-state operating reserve model of aggregate thermostatically-controlled-loads for power system short-term reliability evaluation," *Applied Energy*, vol. 241, pp. 46-58, Mar. 2019.

[18] Z. Li, S. Su, X. Jin *et al*., "Stochastic and distributed optimal energy management of active distribution network with integrated office buildings," *CSEE Journal of Power and Energy Systems*, doi: 10.17775/CSEEJPES.2021.04510

[19] J. Hong, H. Hui, H. Zhang *et al*., "Distributed control of large-scale inverter air conditioners for providing operating reserve based on consensus with nonlinear protocol," *IEEE Internet of Things Journal*, vol. 9, no. 17, pp. 15847-15857, Sept. 2022.

[20] N. Lu, "An evaluation of the HVAC load potential for providing load balancing service," *IEEE Transactions on Smart Grid*, vol. 3, no. 3, pp. 1263-1270, Sept. 2012.

[21] B. Zeng and L. Zhao, "Solving two-stage robust optimization problems using a column-and-constraint generation method," *Operations Research Letters*, vol. 41, no. 5, pp. 457-461, Jun. 2013.

[22] A. Kargarian and Y. Fu, "System of systems based security-constrained unit commitment incorporating active distribution grids," *IEEE Transactions on Power Systems*, vol. 29, no. 5, pp. 2489-2498, Sept. 2014.

[23] H. Ma and S. M. Shahidehpour, "Unit commitment with transmission security and voltage constraints," *IEEE Transactions on Power Systems*, vol. 14, no. 2, pp. 757-764, May 1999.

Yongli Ji received the B.Sc. degree in electrical engineering and automation from Hohai University, Nanjing, China, in 2016, and the Ph. D. degree in electrical engineering from Southeast University, Nanjing, China, in 2022. She is currently working as an Assistant Professor in Nanjing Institute of Technology, Nanjing, China. Her research interests include power system optimal operation and demand-side management.

Qingshan Xu received the B. Sc. degree in electrical engineering from Southeast University, Nanjing, China, in 2000, the M. Sc. degree in electrical engineering from Hohai University, Nanjing, China, in 2003, and the Ph. D. degree in electrical engineering from Southeast University, Nanjing, China, in 2006, respectively. He is currently working as a Professor in Southeast University. His research interests include renewable energy, power system operation and control, and demand-side management.

Yuanxing Xia received the B.Sc. degree in electrical engineering from Hohai University, Nanjing, China, in 2019. He is currently pursuing the Ph.D. degree in electrical engineering in Southeast University, Nanjing, China. His research interests include energy storage technology and peer to peer (P2P) power transaction.